The stretching of an electrified non-Newtonian jet: A model for electrospinning

J. J. Feng
The Levich Institute for Physicochemical Hydrodynamics, City College of the City University of New York, New York, New York 10031

(Received 7 September 2001; accepted 7 August 2002; published 23 September 2002)

Electrospinning uses an external electrostatic field to accelerate and stretch a charged polymer jet, and may produce ultrafine ''nanofibers.'' Many polymers have been successfully electrospun in the laboratory. Recently Hohman *et al.* [Phys. Fluids, **13**, 2201 (2001)] proposed an electrohydrodynamic model for electrospinning Newtonian jets. A problem arises, however, with the boundary condition at the nozzle. Unless the initial surface charge density is zero or very small, the jet bulges out upon exiting the nozzle in a ''ballooning instability,'' which never occurs in reality. In this paper, we will first describe a slightly different Newtonian model that avoids the instability. Well-behaved solutions are produced that are insensitive to the initial charge density, except inside a tiny ''boundary layer'' at the nozzle. Then a non-Newtonian viscosity function is introduced into the model and the effects of extension thinning and thickening are explored. Results show two distinct regimes of stretching. For a ''mildly stretched'' jet, the axial tensile force in the fiber resists stretching, so that extension thinning promotes stretching and thickening hinders stretching. For a ''severely stretched'' jet, on the other hand, the tensile force enhances stretching at the beginning of the jet and suppresses it farther downstream. The effects of extensional viscosity then depend on the competition between the upstream and downstream dynamics. Finally, we use an empirical correlation to simulate strain hardening typical of polymeric liquids. This generally steepens the axial gradient of the tensile stress. Stretching is more pronounced at the beginning but weakens later, and ultimately thicker fibers are produced because of strain hardening. © *2002 American Institute of Physics.* [DOI: 10.1063/1.1510664]

I. INTRODUCTION

The so-called nanofibers, i.e., fibers with submicron diameters, have a potentially enormous role in nanotechnology, with applications ranging from artificial tissues to nanocomposites and to nanoscale machinery.[1–4] A straightforward method of producing nanofibers is *electrospinning*, where electrostatic forces on a charged polymer jet elongates it into thin fibers before solidification. The first patents on electrospinning were filed in the 1930s, but its significance for making nanofibers was recognized only recently during the upsurge of nanotechnology. To date, many polymers have been electrospun in the laboratory, either in melt or solution, including biopolymers, electrically conducting polymers, and liquid–crystalline polymers.[2] In comparison, theoretical studies of electrospinning are few.

Electrospinning typically involves two stages. In the first, a polymer jet issues from the nozzle and is accelerated and stretched smoothly by electrostatic forces. In the second stage, a ''bending instability'' occurs farther downstream when the jet gets sufficiently thin, and the fiber spirals violently. The enormously increased contour length produces a very large stretch ratio and a nanoscale diameter. For the steady stretching in stage one, Spivak and Dzenis[5] published a simple model that assumes the electric field to be uniform and constant, unaffected by the charges carried by the jet. Hohman *et al.*[6,7] developed a slender-body theory for electrospinning that couples jet stretching, charge transport, and the electric field. The model encounters difficulties, however, with the boundary condition at the nozzle. Steady solutions may be obtained only if the surface charge density at the nozzle is set to zero or a very low value. Even after this drastic assumption, no steady solution was possible for fluids with higher conductivities. For stage two, the bending instability has been carefully documented by two groups (Reneker *et al.*;[8,9] Shin *et al.*[10]); each has proposed a theory for the instability. Reneker *et al.* modeled the polymer jet by a linear Maxwell equation. Like-charge repulsion generates a bending force that destabilizes the jet. Hohman *et al.*[6] built an electrohydrodynamic instability theory, and predicted that under favorable conditions, a nonaxisymmetric instability prevails over the familiar Rayleigh instability and a varicose instability due to electric charges. In theoretical work to date, the rheology of the polymer jet has been represented by a Newtonian viscosity,[6,7] a power-law viscosity,[5] and the linear Maxwell equation.[8,9]

This paper concerns the first stage only. The steady-stretching process is important in that it not only contributes to the thinning directly, but also sets up the conditions for the onset of the bending instability. Our objective is twofold. First, we wish to clarify the problems with the Newtonian model of Hohman *et al.*[7] As will be detailed in Secs. II and III, the ballooning instability can be eliminated if the calculation of the electric field is *simplified* in the Hohman *et al.*

formulation. The simplified model will be tested by comparing its predictions with experimental data for various boundary conditions and parameter values. Second, we explore the effects of a non-Newtonian extensional viscosity in electrospinning. As is intuitively expected and confirmed by experiments,[8] the axial tensile force along the fiber is critical to its stretching and stability. To fit the data, previous models had to use an extremely high constant extensional viscosity.[8] This is, of course, indicative of the strong dependence of the extension viscosity on the strain and strain rate for polymeric liquids. In Sec. IV, we will explore the effects of extension thinning, extension thickening, and strain hardening on jet stretching. These results will form the basis for a more rigorous analysis of the role of viscoelasticity in electrospinning.

II. SLENDER-BODY THEORY

In electrospinning, the jet is elongated by electrostatic forces and gravity, while surface tension, viscosity, and inertia also play a part. As the jet thins, the surface charge density σ varies, which in turn affects the electric field $\mathbf{E}$ and the pulling force. The flow field and $\mathbf{E}$ field are thus intimately coupled. We assume the liquid is weakly conducting so the ''leaky dielectric model'' applies (see Saville[11]). Thus, the jet carries electric charges only on its surface; any charges in the interior are quickly conducted to the surface. Meanwhile, the fluid is sufficiently dielectric so as to sustain an electric field tangential to the jet surface. We will use MKS units for electric properties.

The slender-body approximation is a familiar concept in dealing with jets and drops. It has been widely used in fiber spinning of viscoelastic liquids (e.g., Denn *et al.*[12]) and in electrospraying (e.g., Ganan-Calvo[13]). We make the standard assumptions for slender jets: that the jet radius R decreases slowly along the axial direction z: $|dR(z)/dz| \ll 1$, and that the axial velocity v is uniform in the cross section of the jet. Thus, we have simplified the flow to a nonuniform elongation, with all quantities depending only on the axial position z.

A. Governing equations

The jet is governed by four steady-state equations representing the conservation of mass and electric charges, the linear momentum balance, and Coulomb's law for the $\mathbf{E}$ field.

Mass conservation requires that

$$\pi R^2 v = Q, \tag{1}$$

where Q is a constant volume flow rate. Charge conservation may be expressed by

$$\pi R^2 K E + 2\pi R v \sigma = I, \tag{2}$$

where E is the z component of the electric field, K is the conductivity of the liquid, and I is the constant total current in the jet. The momentum equation is formulated by considering the forces on a short segment of the jet (Fig. 1):

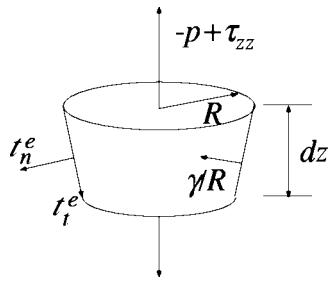

FIG. 1. Momentum balance on a short section of the jet.

$$\frac{d}{dz}(\pi R^2 \rho v^2) = \pi R^2 \rho g + \frac{d}{dz}[\pi R^2(-p+\tau_{zz})] + \frac{\gamma}{R}\cdot 2\pi R R' + 2\pi R(t_t^e - t_n^e R'), \tag{3}$$

where τ_{zz} is the axial viscous normal stress, p is the pressure, γ is the surface tension, and t_t^e and t_n^e are the tangential and normal tractions on the surface of the jet due to electricity. The prime indicates derivative with respect to z, and R' is the slope of the jet surface. The ambient pressure has been set to zero. The electrostatic tractions are determined by the surface charge density and the electric field:[11]

$$t_n^e = \left\| \frac{\epsilon}{2}(E_n^2 - E_t^2) \right\| \approx \frac{\sigma^2}{2\bar{\epsilon}} - \frac{\bar{\epsilon}-\epsilon}{2}E^2, \tag{4}$$

$$t_t^e = \sigma E_t \approx \sigma E, \tag{5}$$

where ϵ and $\bar{\epsilon}$ are the dielectric constants of the jet and the ambient air, respectively, E_n and E_t are the normal and tangential components of the electric field at the surface, and $\|*\|$ indicates the jump of a quantity across the surface of the jet. We have used the jump conditions for E_n and E_t: $\|\epsilon E_n\| = \bar{\epsilon}\bar{E}_n - \epsilon E_n = \sigma$, $\|E_t\| = \bar{E}_t - E_t = 0$, and assumed that $\epsilon E_n \ll \bar{\epsilon}\bar{E}_n$ (see Ganan-Calvo[13]) and $E_t \approx E$. The overbar indicates quantities in the surrounding air.

The pressure $p(z)$ is determined by the radial momentum balance, and applying the normal force balance at the jet surface leads to

$$-p + \tau_{rr} = t_n^e - \frac{\gamma}{R}. \tag{6}$$

Inserting Eqs. (4)–(6) into Eq. (3) yields

$$\rho v v' = \rho g + \frac{3}{R^2}\frac{d}{dz}(\eta R^2 v') + \frac{\gamma R'}{R^2} + \frac{\sigma\sigma'}{\bar{\epsilon}} + (\epsilon - \bar{\epsilon})EE' + \frac{2\sigma E}{R}, \tag{7}$$

where a generalized Newtonian constitutive relation has been used for the viscous normal stress difference:

$$\tau_{zz} - \tau_{rr} = 3\eta v', \tag{8}$$

and the viscosity η may depend on the local strain rate or the accumulated strain (see Sec. IV).

The momentum equation (7) is essentially the same as that in Ganan-Calvo[13] and Hohman *et al.*[6] The latter authors used a more formal procedure of series expansion. The intui-

tive control-volume balance used here corresponds to the leading order of the expansion.[14,15] Spivak and Dzenis'[5] momentum equation misses several terms: the viscous normal stress t_{rr}; the surface tension term in the z equation (though it is included in the r equation); and the normal electrostatic traction t_n^e in both axial and radial balances. Those terms are not, in general, smaller than the terms retained.

Finally, the electric potential inside the jet is determined by the free and induced charges on the jet surface. The induced charges are determined by E_n and $\bar{E}_n$: $\sigma_{\text{ind}}=(\epsilon-\epsilon_0)E_n-(\bar{\epsilon}-\epsilon_0)\bar{E}_n$, where ϵ_0 is the permittivity of vacuum. The normal field E_n is related, via Gauss' law, to the axial field E:

$$2\pi RE_n+\frac{d}{dz}(\pi R^2E)=0.$$

Since $\bar{\epsilon}\bar{E}_n-\epsilon E_n=\sigma$, $\bar{E}_n$ can also be expressed in terms of E. Now the potential along the centerline of the jet, due to the total surface charges $\sigma+\sigma_{\text{ind}}$, may be obtained by Coulomb's law:

$$\phi(z)=\phi_\infty(z)+\frac{1}{2\bar{\epsilon}}\int\frac{\sigma R\,d\zeta}{\sqrt{(z-\zeta)^2+R^2}}-\frac{\beta}{4}\int\frac{d(ER^2)/d\zeta}{\sqrt{(z-\zeta)^2+R^2}}d\zeta, \tag{9}$$

where ϕ_∞ is the potential due to the *external* field in the absence of the jet, $\beta=\epsilon/\bar{\epsilon}-1$, and the integration is over the entire length of the fiber L. To avoid solving an integrodifferential equation, one realizes that the dominant contribution to the integrals comes from the two regions satisfying $R\ll|z-\zeta|\ll L$. An asymptotic estimation leads to (cf. Hinch[16])

$$\phi(z)\approx\phi_\infty(z)+\ln\chi\left(\frac{1}{\bar{\epsilon}}\sigma R-\frac{\beta}{2}\frac{d(ER^2)}{dz}\right),$$

where the aspect ratio $\chi=L/R_0$, R_0 being the characteristic radius of the jet. The axial field is, therefore,

$$E(z)=E_\infty(z)-\ln\chi\left(\frac{1}{\bar{\epsilon}}\frac{d(\sigma R)}{dz}-\frac{\beta}{2}\frac{d^2(ER^2)}{dz^2}\right). \tag{10}$$

From this point on, we will take the external field E_∞ to be spatially uniform. Equations (9) and (10) have been previously derived by Hohman *et al.*[6] by using the idea of an effective line charge along the axis of the jet. Spivak and Dzenis[5] neglected the axial field due to surface charges and assumed a constant $E=E_\infty$ everywhere. This will be seen to be a poor approximation since $E(z)$ typically varies greatly.

Now we have Eqs. (1), (2), (7), and (10) for the four unknown functions R, v, E, and σ. These are similar to those used in the electrospray literature,[13] and are essentially the same as those derived by Hohman *et al.*[6] To achieve better agreement with experimental data, however, Hohman *et al.*[7] used a more sophisticated method to compute E. First, Eq. (9) is not reduced to Eq. (10). To account for the capacitor plates in the experiment and the protruding nozzle, image charges are added to the integrodifferential equation, as is a "fringe field" due to the charged nozzle. Interestingly, the more complex model suffers from a difficulty with the boundary condition at the origin of the jet, while the simpler model does not. This puzzle will be further investigated in Sec. II C as related to the boundary conditions.

B. Dimensionless parameters

Parameters in electrospinning fall into three categories: process parameters (Q, I, and E_∞), geometric parameters (R_0 and L), and material parameters (ρ, η_0, ϵ, $\bar{\epsilon}$, K, and γ). Among those, R_0 is the radius at the origin of the jet just outside the nozzle, and η_0 is the zero-shear-rate viscosity. We adopt the following characteristic quantities:

Length: R_0;
velocity: $v_0=Q/(\pi R_0^2)$;
electric field: $E_0=I/(\pi R_0^2K)$;
surface charge density: $\sigma_0=\bar{\epsilon}E_0$.

Scaling all quantities using these characteristic values, and denoting the dimensionless quantities using the same symbols, we arrive at the following dimensionless governing equations:

$$R^2v=1, \tag{11}$$

$$ER^2+\text{Pe}\,Rv\sigma=1, \tag{12}$$

$$vv'=\frac{1}{\text{Fr}}+\frac{3}{\text{Re}}\frac{1}{R^2}\frac{d(\eta R^2v')}{dz}+\frac{1}{\text{We}}\frac{R'}{R^2}+\mathcal{E}\left(\sigma\sigma'+\beta EE'+\frac{2E\sigma}{R}\right), \tag{13}$$

$$E=E_\infty-\ln\chi\left(\frac{d(\sigma R)}{dz}-\frac{\beta}{2}\frac{d^2(ER^2)}{dz^2}\right), \tag{14}$$

where the dimensionless groups are the following:

Electric Peclet number: $\text{Pe}=\dfrac{2\bar{\epsilon}v_0}{KR_0}$,

Froude number: $\text{Fr}=\dfrac{v_0^2}{gR_0}$,

Reynolds number: $\text{Re}=\dfrac{\rho v_0R_0}{\eta_0}$,

Weber number: $\text{We}=\dfrac{\rho v_0^2R_0}{\gamma}$,

aspect ratio: $\chi=\dfrac{L}{R_0}$,

$\mathcal{E}=\dfrac{\bar{\epsilon}E_0^2}{\rho v_0^2}$,

$\beta=\dfrac{\epsilon}{\bar{\epsilon}}-1$.

Note, in particular, that Pe indicates the importance of charge convection relative to conduction, $\mathcal{E}$ indicates the magnitude of the electrostatic forces relative to inertia, and β represents the significance of induced charges. We have taken the cur-

rent I to be an independent parameter. In reality, I depends on a host of factors—including details of the setup—in ways that are poorly understood. For instance, drastically different current–voltage relationships have been reported for electrospraying[23] and electrospinning[7] experiments. In this paper, we use measured I values when comparing with experiments.

C. Boundary conditions

Mass and charge conservations allow v and σ to be expressed in terms of R and E, and the momentum and E-field equations can be recast into two second-order ordinary differential equations for R and E, each requiring two boundary conditions. At the origin of the jet ($z=0$), an obvious condition is

$$R(0)=1. \tag{15}$$

We have assumed that the slender-body theory applies up to the nozzle, though conceivably the slope $|R'|$ may not be small there. The same assumption has been used in most previous models concerning jets or drops. For Newtonian fluids, Eggers and Dupont[17] used a one-dimensional model to compute the detachment of a drop from an orifice, and Zhang *et al.*[18] simulated the stretching and breakup of a liquid bridge. In both cases, the predictions are in excellent agreement with experimental measurements, even though $|R'|$ appears to be rather large in certain areas of the jet and drop. Keunings *et al.*[19] carried out two-dimensional finite-element simulations of fiber spinning for Newtonian and Maxwell fluids. Their results confirmed that it is acceptable to use the conditions at the nozzle as entrance boundary conditions for the slender-body model.[20]

At the "exit," we apply the asymptotic thinning conditions due to Kirichenko *et al.*[21] Specifically, as R and σ drop to zero and E approaches E_∞, the stretching of the jet is governed by a balance among inertia, gravity, and tangential electrostatic force. This leads to the asymptotic scaling $R(z)\propto z^{-1/4}$. Hence, we adopt the following exit conditions at $z=\chi$:

$$R+4zR'=0, \tag{16}$$

$$E=E_\infty. \tag{17}$$

Note that if the straight jet is followed by the spiraling instability, the latter may modify the exit conditions for the straight portion of the jet. This possible complication is not considered in our model.

The fourth boundary condition concerns the surface charge density at the entrance $\sigma(0)$, which, through charge conservation, determines $E(0)$ for any given current I. This is the condition that has caused much difficulty in the Hohman model.[7] In reality, the geometric details of the device and the imposed external field determine $\sigma(0)$. Since such details are not contained in the models, an *ad hoc* condition needs to be introduced. In fact, this has been a long-standing problem in previous studies of electrospraying. Ganan-Calvo[13] and Hartman *et al.*,[22] for instance, circumvented the $\sigma(0)$ condition by specifying the slope $R'(0)$. This introduces the question of where the origin $z=0$ is on the actual jet, and hence difficulties in comparing with experiments. Hohman *et al.*[7] took the pragmatic route of determining $\sigma(0)$ by fitting model predictions to measurements. The surprising outcome is that steady solutions are attainable only if $\sigma(0)$ is zero or very small. Otherwise, the jet would bulge into a balloon soon after exiting the nozzle. For liquids with higher conductivity, even $\sigma(0)=0$ cannot prevent a long-wave instability of the jet, in contradiction to observations.

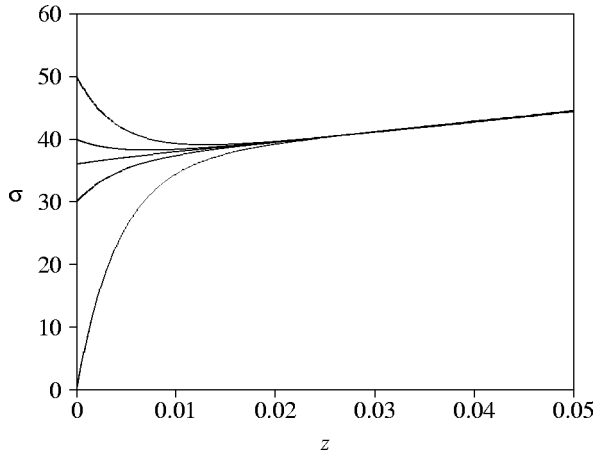

FIG. 2. The boundary layer at the origin of the jet predicted by our model. For the different $\sigma(0)$ values used (0, 30, 36, 40, 50), the solution is essentially the same for $z>z_{\mathrm{BL}}=0.02$. Note that σ is made dimensionless by $\sigma_0=\overline{\epsilon I}/(\pi R_0^2 K)$ and z by the initial radius R_0.

We solved our model equations for a wide range of $\sigma(0)$ values and different conductivities and found neither of the problems. In fact, $\sigma(0)$ only modifies the $\sigma(z)$ profile within a tiny "boundary layer:" $0<z\leqslant z_{\mathrm{BL}}$. For $z>z_{\mathrm{BL}}$, the solution is practically independent of $\sigma(0)$ (Fig. 2). This is reminiscent of conventional fiber spinning, where the normal stress boundary condition $\tau_{rr}(0)$ has to be specified *ad hoc* but turns out to have little effect on the solution.[12] Then $\tau_{rr}(0)=0$ is used since it would otherwise drop to zero outside the boundary layer. Following this example, we specify our $\sigma(0)$ according to the slope of $\sigma(z)$ outside the boundary layer. The rationale for this choice is that a sharp gradient is unlikely in a real jet. Figure 2 also suggests that $\sigma(0)$ is not a free parameter in reality but should be determined by some physical constraint not incorporated in the theory.

It is astonishing that the more sophisticated model of Hohman *et al.*[7] suffers from the unrealistic ballooning instability while our model does not, as the latter derives from the former when the integrodifferential equation (9) is approximated by the ordinary differential equation (10). To explain this paradox, we note that the electric potential due to a charged slender body may be written as in Eq. (9) only if $R(z)$ is continuous and *vanishes at both ends*.[16] The latter condition is clearly violated in this situation. Since σ and R both approach zero downstream, the thinner end (i.e., the exit) contributes nothing to the electric field. The upstream end, on the other hand, does affect the electric field. In other words, our "slender" jet does not end at the spinneret, and Eq. (9) ignores the effects of the charges carried by the polymer and the spinneret *upstream* of the nozzle. Thus, the axial

field is underestimated and radial repulsion of the charges gives rise to the ballooning instability.

In an effort to account for some of the upstream effects, Hohman *et al.*[7] added two more features to Eq. (9): image charges due to the two equipotential capacitor plates and a fringe field due to the protruding nozzle. Though these refinements increase the axial field, enhance stretching of the jet and bring the thinning curve $R(z)$ closer to measurements, they do not address the fundamental defect of Eq. (9). Ganan-Calvo[23] rejected the picture of a slender jet extending up to the nozzle. Instead, he constructed a local asymptotic solution for a slender jet attached to a Taylor cone. The electric current thus predicted depends on neither the imposed voltage nor the dielectric constant of the jet. This general result is supported by electrospraying experiments but does not agree with electrospinning experiments,[7,24,25] again highlighting the importance of details of the experimental setup.

In this light, the replacement of Eq. (9) by Eq. (10) is a pragmatic approach that avoids the need to account for the effects of upstream charges or details of the device. This way, the slender-body theory can be applied up to the nozzle. The tradeoff is that an additional boundary condition, $E(0)$ or $\sigma(0)$, has to be specified. Then the boundary layer (cf. Fig. 2) offers an *ad hoc* representation of the actual physics near the nozzle. In the next section, we will examine the capability of the Hohman *et al.* model and our simplified version in predicting experimental data for Newtonian jets.

III. NEWTONIAN JETS

A. Comparison with experiment

Among experimental studies of electrospinning, the measurements of Hohman *et al.*[7] are the most comparable to our model. Two liquids are used: glycerol and an aqueous poly(ethylene oxide) (PEO) solution. Hohman *et al.* compared predictions of their theory with measurements only for glycerol; no steady theoretical solution was possible for PEO because of its relatively high conductivity. We will compare the predictions of our model in Eqs. (11)–(14), with proper boundary conditions and parameter values, with the measurements and predictions of Hohman *et al.*

Hohman *et al.* give the following parameter values for a typical glycerol jet: $R_0=0.08$ cm, $L=6$ cm, $Q=1$ mL/min, $E_\infty=5$ kV/cm, $I=170$ nA, kinematic viscosity $\nu=14.9$ cm^2/s, $K=0.01$ μS/cm. Additional parameters are found in handbooks (e.g., Ref. 26): $\gamma=63.4$ dyne/cm, $\rho=1.26\times10^3$ kg/m^3, $\bar{\epsilon}=8.854\times10^{-12}$ C^2/N m^2, and $\epsilon/\bar{\epsilon}=46.5$. Now the dimensionless parameters are $\chi=75$, $\beta=45.5$, $\mathrm{Re}=4.451\times10^{-3}$, $\mathrm{We}=1.099\times10^{-3}$, $\mathrm{Fr}=8.755\times10^{-3}$, $\mathrm{Pe}=1.835\times10^{-4}$, $\mathcal{E}=0.7311$, and $E_\infty=5.914$.

Using these parameters, we integrated our ordinary differential equations by a relaxation method on a nonuniform grid.[27] The result is compared with the Hohman results in Fig. 3. Apparently, our model grossly overpredicts jet thinning (curve *a*). To explain this discrepancy, we note that two of the parameter values listed above differ from those in the literature. First, all sources we found list the *dynamic* viscosity as 14.9 P at 20 °C, corresponding to a kinematic viscosity of 11.8 cm^2/s, smaller than that used by Hohman *et al.* Using the lower viscosity increases the Reynolds number to $\mathrm{Re}=5.608\times10^{-3}$, resulting in a minor *increase* in stretching (curve *b*). Second, a wide range of values have been reported for the conductivity K in the literature,[28–30] ranging from 1.6×10^{-6} to 9×10^{-6} S/m at room temperature. This scatter is perhaps attributable to the hygroscopicity of glycerol, but all values are higher than that used by Hohman *et al.* In view of this uncertainty, we tested different K values at the higher Re and found that for $K=4.8\times10^{-6}$ S/m, our model produces an almost perfect agreement with the measured jet (curve *c*). The effect of K on jet stretching is easy to interpret: a higher K causes surface charges to conduct more readily downstream, hence reducing the charge density σ and the electrostatic force responsible for stretching the jet. In the context of our model, a higher K corresponds to a lower $\mathcal{E}$ and hence reduced electrostatic effect on the jet.

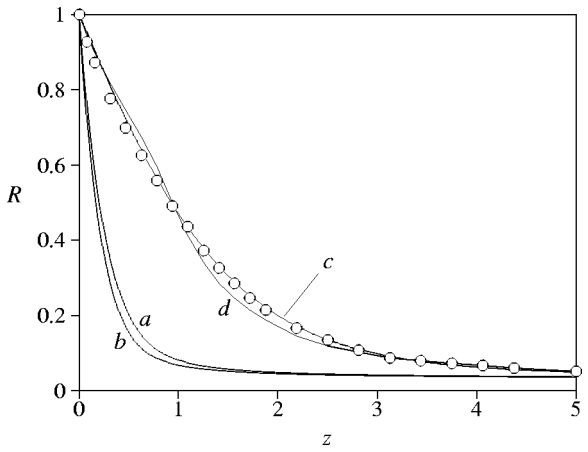

FIG. 3. A comparison between predictions of our simplified model and the theoretical and experimental results of Hohman *et al.* (Ref. 7) for a glycerol jet. (a) Our prediction using the parameters of Hohman *et al.*: $\chi=75$, $\beta=45.5$, $\mathrm{Re}=4.451\times10^{-3}$, $\mathrm{We}=1.099\times10^{-3}$, $\mathrm{Fr}=8.755\times10^{-3}$, $\mathrm{Pe}=1.835\times10^{-4}$, $\mathcal{E}=0.7311$, and $E_\infty=5.914$. (b) Our model prediction at a slightly higher $\mathrm{Re}=5.608\times10^{-3}$. (c) Our model prediction using a higher conductivity $K=4.8\times10^{-6}$ S/m, corresponding to $\mathrm{Pe}=3.823\times10^{-5}$, $\mathcal{E}=3.173\times10^{-2}$, and $E_\infty=28.32$. (d) Model prediction of Hohman *et al.* using the parameters of curve (a). The data points represent the experimentally measured thinning curve.

Figure 4 compares the E and σ profiles predicted by the two models for the glycerol jet. The E curves have the same general shape. The σ curve of Hohman *et al.*, however, has irregular wiggles near $z=0$, indicating the solution is poorly converged. Furthermore, σ jumps from 0 to a finite value of about 4×10^{-5} C/m^2 almost instantaneously. (The curve was read off Fig. 10 of Ref. 7 in which the σ curve appears to intersect $z=0$ at roughly 12 esu/cm^2 rather than 0.) In addition, Hohman *et al.*[7] suggested that $\sigma(0)=0$ may be physically reasonable since the charges would not have enough time to relax onto the surface at the nozzle. Then it would be hard to explain the initial jump in σ since nothing else has changed in such a short distance. Also shown in Fig. 4 are E and σ profiles obtained by applying a ''universal scaling'' for electrospraying experiments[31] to our parameters. The electrospraying profiles differ markedly from the electrospinning models, except for the humped shape. This is not surprising since the current–voltage relationship is very different in the

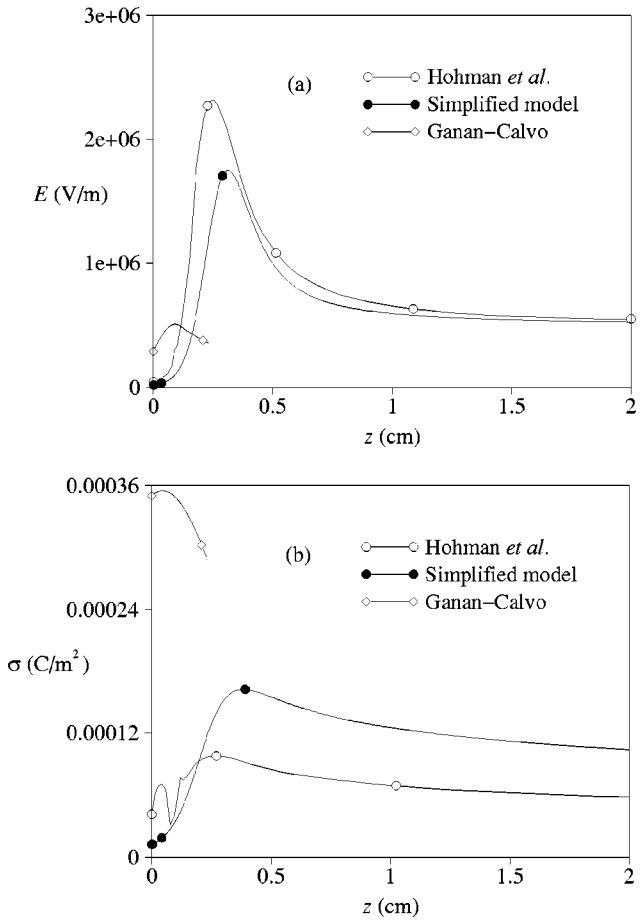

FIG. 4. A comparison of the predictions of the two models for (a) E and (b) σ. Different parameter values, corresponding to curve (c) and (d) in Fig. 3, are used for the simplified model and the Hohman model, respectively. Also shown are profiles obtained by applying the universal scaling of Ganan-Calvo (Ref. 31) to the parameters of curve (c) in Fig. 3.

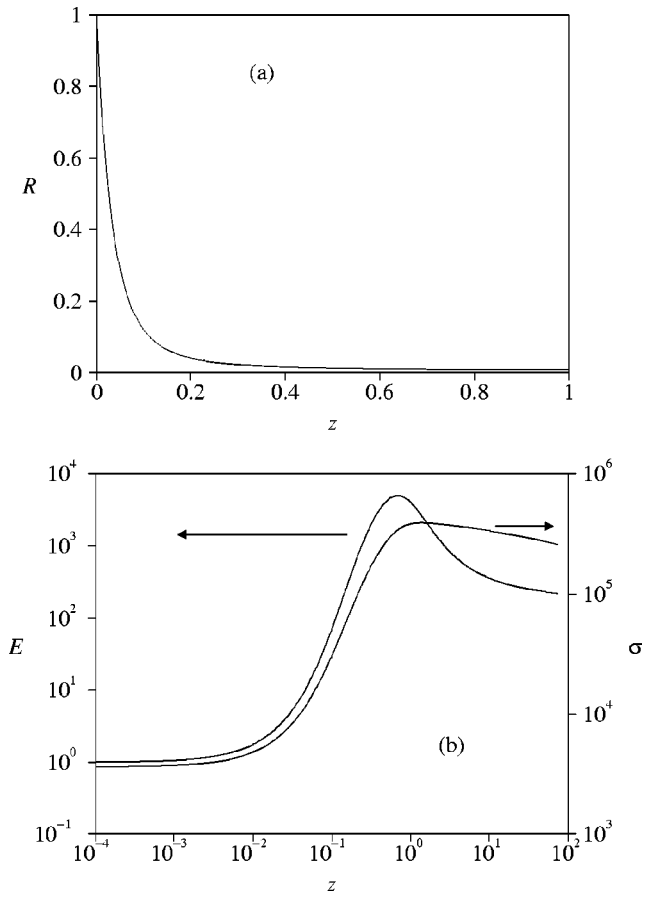

FIG. 5. Predictions of our simplified model using parameters for the PEO jet. (a) The thinning curve $R(z)$. Most of the stretching occurs within a distance of less than one initial radius from the nozzle; (b) E and σ increase by two to three orders of magnitude within this short distance.

two operations,[7] owing probably to differences in details of geometric setup and operational conditions.

Figure 5 plots the predictions of our model using parameters corresponding to the PEO jets in the experiment of Hohman *et al.* The high conductivity and strong current lead to very high levels of surface charge near the nozzle and a local E field almost 100 times higher than E_∞. The consequence is extremely severe initial thinning of the jet. In dimensional terms, the initial thinning rate $|R'|$ and the maximum values of E and σ are all one order of magnitude higher than the glycerol jet in Figs. 3 and 4. Hohman *et al.* did not present quantitative experimental data for the PEO jet, so direct verification of our predictions is not possible. But in contrast to the Hohman model, our model at least produces well-behaved solutions for high-K, high-I electrospinning.

B. Effects of dimensionless parameters

Before applying our simplified model to non-Newtonian fluids, we further investigate the Newtonian solutions by examining the effects of the dimensionless parameters. This is accomplished by using the solution depicted in Fig. 3 (curve *c*) and Fig. 4 (corresponding to $K=4.8\times10^{-6}$ S/m) as the *base*, and varying the parameters one at a time.

The qualitative features of the solution stay the same when the parameters are varied by two orders of magnitude about their base values. We will analyze these basic features first. The rate of thinning $|R'|$ is maximum at $z=0$, and then relaxes smoothly downstream toward zero (cf. Fig. 3). Downstream of the origin, both E and σ shoot up to a peak and then relax; the maxima typically occur within five initial radii but do not coincide (cf. Fig. 4). To understand these features, we realize that the thinning of the jet and the variations in E and σ are all interconnected. Mathematically, Eq. (12) implies $\sigma'=(1-3ER^2)R'/\mathrm{Pe}-E'R^3/\mathrm{Pe}\approx-2R'/\mathrm{Pe}$ since $ER^2\approx1$ for the small Pe used here and E' is typically very small at the start of the jet. Hence, $\sigma'\gg0$ and the sharp rise in σ can be explained. Physically, the shrinking cross section reduces the amount of charges that can be conducted. To maintain the same current, convection has to carry more charges. Given the low jet speed near the nozzle, the charge density surges. The electric field E is induced by the axial gradients of surface charges $(\sigma R)'$ and induced charges $(ER^2)''$. For the parameters tested, the former dominates and may be estimated as $(\sigma R)'\approx-2RR'/\mathrm{Pe}$. Equation (14) then leads to $E'\approx\ln\chi(R^2)''/\mathrm{Pe}$, which is a large positive number for *convex* thinning curves (cf. Fig. 3). Hence, E jumps up. As the jet gets thinner and faster, electric conduction gradually gives way to convection. Toward the end, Eq. (12) re-

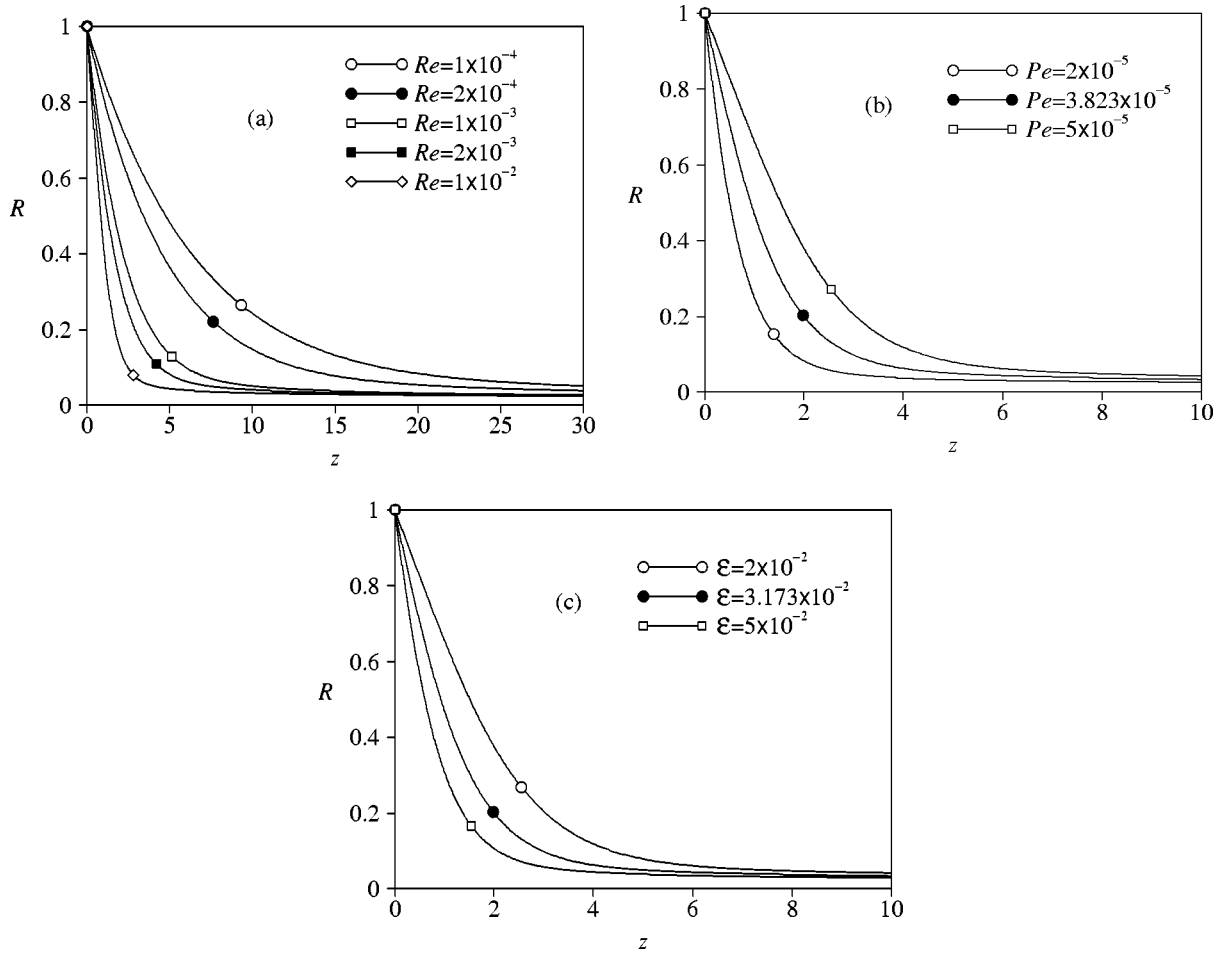

FIG. 6. Effects of the dimensionless parameters (a) Re, (b) Pe, and (c) $\mathcal{E}$ on the Newtonian jet. Each parameter is varied alone with the others fixed at the base values: $\chi=75$, $\beta=45.5$, $\mathrm{Re}=5.608\times10^{-3}$, $\mathrm{We}=1.099\times10^{-3}$, $\mathrm{Fr}=8.755\times10^{-3}$, $\mathrm{Pe}=3.823\times10^{-5}$, $\mathcal{E}=3.173\times10^{-2}$, and $E_\infty=28.32$.

quires $\sigma\approx(\mathrm{Pe}\,Rv)^{-1}=R/\mathrm{Pe}$ to decrease with R. As the surface charges diminish, $E\to E_\infty$ and the asymptotic behavior emerges. With this qualitative picture in hand, we will examine next the quantitative changes due to the various parameters.

As expected, gravity enhances stretching while surface tension opposes it. But both effects are weak for our range of parameters. Reducing Fr or We by a factor of 10 brings about roughly a 5% change in R. Another relatively insignificant parameter is β, which represents the magnitude of induced charges. In terms of the electric field E [Eq. (14)], the induced charges contribute roughly 1% of the total field and thus is overwhelmed by the free charges. Repulsion among the induced charges enhances stretching of the jet through the $\beta\mathcal{E}EE'$ term in Eq. (13). Increasing β from 1 to 100 causes up to a 20% decrease in R for the base parameters used here.

Perhaps anti-intuitively, the solution is also insensitive to E_∞. Much of the thinning occurs near the beginning of the jet, where E can be an order of magnitude higher than E_∞. Evidently, the strong E field is induced *locally* by the surface charges on the jet, and has little to do with the ''external'' field E_∞. Hence, varying E_∞ with other parameters fixed has little influence on the solution. However, the physical intuition that the external field should to a large extent determine jet stretching is still correct. In reality, raising the field strength also raises the current I, more or less linearly (cf. Fig. 4 of Hohman *et al.*[7]). Then the characteristic field $E_0=I/(\pi R_0^2K)$ increases in proportion and the dimensionless E_∞ would change little. It is $\mathcal{E}$ that will reflect the increase in the electrostatic pull due to the elevated *dimensional* E_∞.

Figure 6 depicts the effects of Re, Pe, and $\mathcal{E}$. Increasing Re promotes stretching of the jet [Fig. 6(a)], as has been noticed in Fig. 3. Re appears in the momentum equation [Eq. (13)] only, and exerts its impact via the gradient of the axial tensile force $T=(\tau_{zz}-\tau_{rr})R^2=3\,\eta v'R^2$. The variation of T along the jet can be nonmonotonic, however, meaning the viscous normal stress may promote or resist stretching in a different part of the jet and under different conditions. Thus, the effect of Re is rather subtle. We postpone a detailed analysis to the next section (see Fig. 10). Increasing Pe reduces jet stretching, and the effect has a straightforward explanation [Fig. 6(b)]. Charge conservation [Eq. (12)] implies that σ decreases with increasing Pe, other conditions being fixed. In experimental terms, increasing Pe alone can be achieved by reducing K and I simultaneously, giving rise to lower surface charge density σ. The result is a weaker electrostatic pulling force on the jet and reduced stretching. The solution for PEO in Fig. 5 illustrates how a low Pe value (due mainly to the higher K and I) boosts stretching. Finally,

since $\mathcal{E}$ denotes the ratio of electric to inertial forces, increasing $\mathcal{E}$ promotes stretching in Fig. 6(c) as one may expect from Eq. (13).

To summarize our study of Newtonian jets, the difficulty in modeling electrospinning and electrospraying is to account for the upstream effects on the **E** field. Not having accomplished this, the model of Hohman *et al.*[7] fails near the nozzle in the form of the ballooning instability. Our simplified model avoids the difficulty at the cost of introducing an extra boundary condition. This leads to a thin boundary layer at the nozzle. Away from the nozzle, both models predict the qualitative trend very well, and may even claim quantitative agreement (we must note that Fig. 3 is complicated by the uncertainty in K). Therefore, we will use the simplified model as a platform for exploring the effects of non-Newtonian rheology on electrospinning.

IV. NON-NEWTONIAN JETS

It is well known that polymeric and Newtonian liquids exhibit a maximal difference in elongation.[32] Two aspects of this rheological difference are especially relevant to electrospinning. When stretching a polymeric liquid from rest, the transient extensional viscosity $\overline{\eta}^{+}$ shoots up with strain, as the polymer molecules uncoil, producing a large transient Trouton ratio, which, for dilute solutions, can be in the thousands.[33] This is commonly known as *strain hardening*. In the event that a steady state is attained, the steady elongational viscosity $\overline{\eta}$ may decrease or increase with the steady stretching rate, creating *extension thinning* or *extension thickening*, respectively. Strain hardening reflects the memory of the liquid and is thus a viscoelastic behavior. Extension thinning or thickening, on the other hand, can be seen as purely viscous and is representable by a generalized Newtonian viscosity.

Like conventional fiber spinning, electrospinning is neither a startup of elongation from rest nor a steady extension in the Lagrangian sense. A fluid particle exits the spinneret with a certain strain history, and then experiences an approximately uniaxial extension with a time-dependent strain rate. To simplify the picture, we will explore the viscous and elastic aspects of extensional rheology separately. First, we disregard strain hardening altogether and assume that the polymer experiences roughly steady-state stretching everywhere at the *local* strain rate. This corresponds to the small Deborah-number limit, and the viscous reaction of the liquid is then described by a thinning or thickening extensional viscosity. Second, we represent strain hardening approximately by using a transient Trouton ratio that depends only on the total strain up to that point. This is, of course, an *ad hoc* approach that allows us to incorporate the memory effect without using complex viscoelastic constitutive equations. Since no steady stretching is achieved, extension thinning or thickening is irrelevant in this case. The two scenarios will be discussed separately in the following.

A. Extension thinning and thickening

Song and Xia[34] proposed a convenient empirical formula to represent extension thinning and/or thickening:

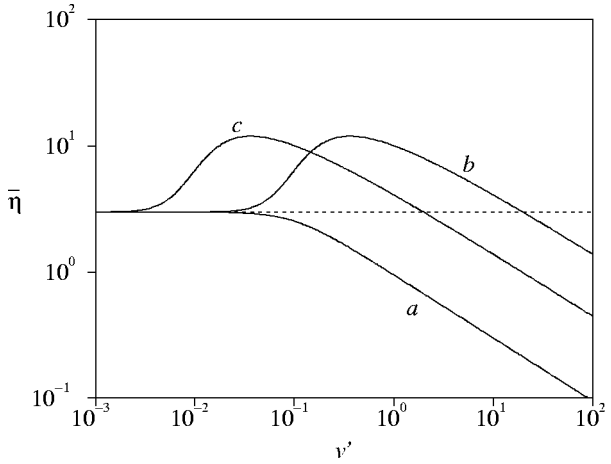

FIG. 7. Typical viscosity curves generated by Eq. (18). The dotted line indicates the Newtonian value of 3, and the asymptotic Trouton ratio is fixed at $\mathrm{Tr}_\infty = 45$. (a) Pure extension thinning with $n = 0.5$, $m = 1$, and $\mathrm{De} = 10$; (b) extension thickening followed by thinning at $n = 0.5$, $m = 0.5$, and $\mathrm{De} = \overline{\mathrm{De}} = 10$; (c) $n = 0.5$, $m = 0.5$, and $\mathrm{De} = \overline{\mathrm{De}} = 100$. The parameter values approximate those determined by fitting the data of Laun and Münsdedt (Ref. 36) for LDPE melts (see Song and Xia (Ref. 34)).

$$\overline{\eta} = \eta_0 \left[1 + \left(\lambda \sqrt{\frac{\mathrm{II}}{2}} \right)^2 \right]^{(n-1)/2} \cdot \mathrm{Tr}(\mathrm{III}),$$

with

$$\mathrm{Tr}(\mathrm{III}) = \mathrm{Tr}_\infty + (3 - \mathrm{Tr}_\infty)(1 + \mu^3 |\mathrm{III}|)^{(m-1)/3},$$

where η_0 is the Newtonian or zero-strain-rate viscosity, II and III are the second and third invariants of the rate-of-strain tensor,[35] Tr_∞ is the asymptotic Trouton ratio at a high strain rate, λ and μ are the relaxation times for shear and extension, and n and m are the corresponding power-law indices. The formula was devised as a universal viscosity for shear, extension, and intermediate flow types. In our context of pure extension, the ''shear-thinning'' part works with the variable Trouton ratio to fit the viscosity curves.

In our nonuniform elongational flow, $\mathrm{II} = 6(dv/dz)^2$, $\mathrm{III} = 6(dv/dz)^3$. The viscosity function can be made dimensionless for use in Eq. (13) in place of 3η:

$$\overline{\eta} = (1 + \mathrm{De}^2 v'^2)^{(n-1)/2} \times [\mathrm{Tr}_\infty + (3 - \mathrm{Tr}_\infty)(1 + \overline{\mathrm{De}}^3 v'^3)^{(m-1)/3}], \quad (18)$$

where the Deborah numbers are defined as $\mathrm{De} = \sqrt{3} v_0 \lambda / R_0$ and $\overline{\mathrm{De}} = \sqrt[3]{6} v_0 \mu / R_0$. Figure 7 plots three typical viscosity curves. Increasing n and m moderates the degree of thinning and thickening; varying the Deborah numbers shifts the curves horizontally and changes the strain rate where thinning or thickening onsets. For the rest of the paper, we will fix $\mathrm{Tr}_\infty = 45$, and assume $\lambda = \sqrt[3]{6}\mu/\sqrt{3}$, so that De and $\overline{\mathrm{De}}$ are always equal.

1. Extension thinning

First, we consider the case of $m = 1$, when Eq. (18) simplifies to a ''shear-thinning'' Carreau viscosity function with a constant Trouton ratio of 3. As mentioned in Sec. III B, when discussing Fig. 6(a), the viscous term in the momen-

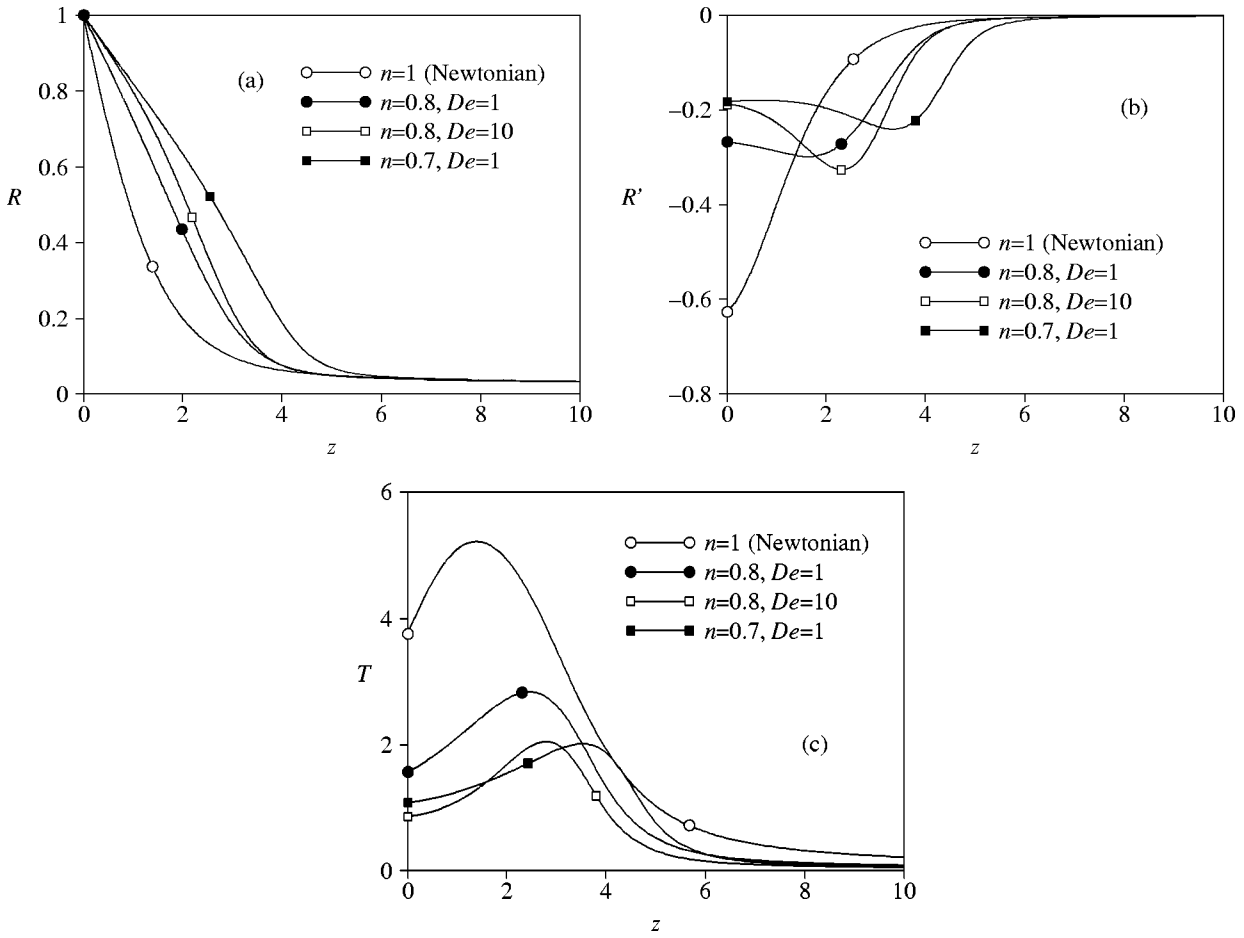

FIG. 8. Stretching is delayed by extension thinning on a severely stretched jet. The parameters are $\chi=75$, $\beta=45.5$, $\mathrm{Re}=5.608\times10^{-3}$, $\mathrm{We}=1.099\times10^{-3}$, $\mathrm{Fr}=8.755\times10^{-3}$, $\mathrm{Pe}=3.823\times10^{-5}$, $\mathcal{E}=3.173\times10^{-2}$, and $E_\infty=28.32$. (a) The radius of the jet R; (b) the stretching rate R'; (c) the tensile force T.

tum equation influences jet stretching in different ways depending on how the tensile force $T(z)$ varies along the jet. In dimensionless terms, we write

$$T=(\tau_{zz}-\tau_{rr})R^2=\overline{\eta}v'R^2=-2\,\overline{\eta}R'/R.$$

Thus, the shape of the $T(z)$ curve depends mainly on how fast $|R'|$ relaxes to zero as R decreases. It is convenient to demarcate two scenarios for *severe* stretching and *mild* stretching depending on whether $T(z)$ has a maximum. For the severely stretched jet, R drops so fast that T initially rises, reaches a peak, and then relaxes downstream. Hence, the viscous normal stress enhances stretching initially $[T'(z)>0]$ but resists it farther downstream $[T'(z)<0]$. For the mildly stretched jet, on the other hand, T decreases monotonically down the jet, and resists stretching everywhere. The variation of T marks a major difference from conventional fiber spinning, where a stretching force is applied only at the wind-up spool, and thus the tensile force remains constant throughout the length of the fiber. This distinction will be seen to strongly affect the stretching of the fiber.

For the severely stretched jet, an extension-thinning viscosity $\overline{\eta}(v')$ causes *delayed stretching*. Figure 8(a) shows that with stronger extension thinning (at a smaller n and/or a higher De), stretching is hampered at the beginning of the jet but intensifies downstream, resulting in more or less the same fiber radius at the end. The delay in stretching is more clearly shown by the stretching rate R' in Fig. 8(b). As is apparent from Fig. 8(c), extension thinning reduces the slope of the initial rise in $T(z)$. This is due to the acceleration of the jet reducing $\overline{\eta}$ outside the nozzle, and explains the weakened initial stretching in Figs. 8(a) and 8(b). Interestingly, the $T(z)$ profiles in Fig. 8(c) resemble the prediction of the theory of Reneker *et al.*[8] using a linear Maxwell model. For the parameters considered, apparently, the humped shape is mainly due to the rate of severe stretching rather than the viscosity $\overline{\eta}$.

To understand how extension thinning causes enhanced stretching farther downstream, we first explain why for Newtonian jets, $|R'|$ is maximum at $z=0$ and relaxes monotonically to zero downstream. The reason the high level of $|R'(0)|$ cannot be sustained downstream, despite the rising E and σ (cf. Fig. 4), lies with the momentum equation [Eq. (13)]. Balancing the acceleration $vv'=-2R'/R^5$ with the electrostatic force on the net charges $2\mathcal{E}\sigma E/R$, we have $|R'|\sim\mathcal{E}\sigma E R^4$. Thus, $|R'|$ has to drop downstream because R^4 decreases too rapidly. Another way of viewing this is that even the rising E and σ cannot maintain the acceleration v' in the face of a rapidly increasing v. All this is changed by

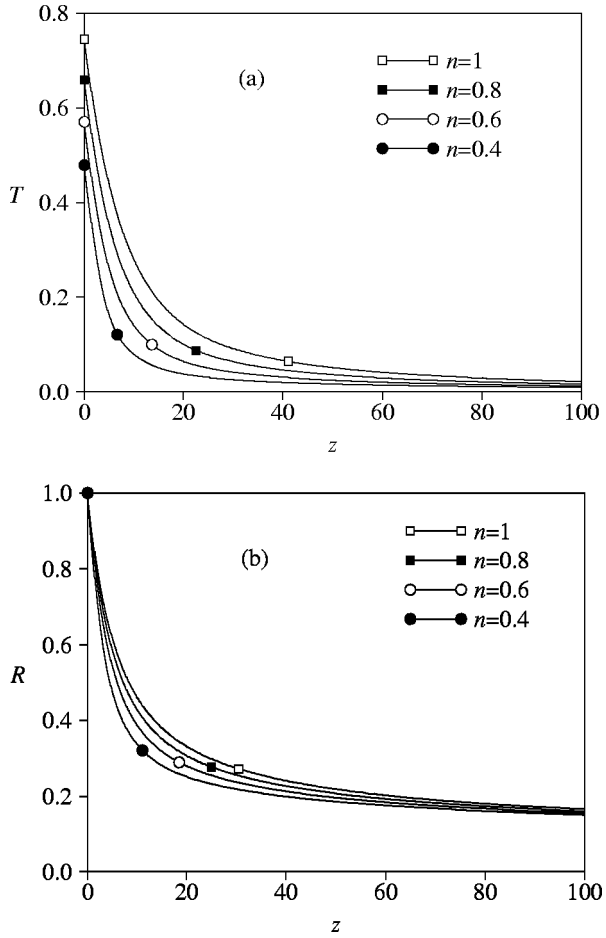

FIG. 9. Extension thinning enhances stretching on a mildly stretched jet. De=10. The other parameters are $\chi=600$, $\beta=40$, Re$=5\times10^{-3}$, We $=0.1$, Fr$=0.1$, Pe$=0.1$, $\mathcal{E}=1$, and $E_\infty=0.1$. (a) Tensile force T; (b) radius R.

extension thinning. As explained before, the initial stretching rate $|R'(0)|$ is reduced by extension thinning and R thins with a milder slope. Then the electric force is able to maintain the initial level of $|R'|$ farther downstream. In the case of more severe extension thinning, the stretching rate even increases downstream to a local maximum before relaxing [cf. Fig. 8(b)]. Thus, the delayed stretching phenomenon occurs. One may notice delayed maxima in $|R'|$, T as well as v', E, and σ (not shown), though the exact positions of the peaks do not coincide.

It is illuminating to contrast the behavior of an extension-thinning jet in electrospinning with that in conventional fiber spinning.[37] In the latter case, T stays constant along z, and the normal stress difference $\tau_{rr}-\tau_{zz}$ increases monotonically downstream as the fiber gets thinner. Consequently, the stretching rate $|R'|$ increases rapidly toward the wind-up spool. $R(z)$ assumes a concave shape, with most of the thinning of the fiber occurring at the spool rather than at the spinneret as in Fig. 8.

The picture is much simpler for the mildly stretched jet. The tensile force $T=-2\overline{\eta}R'/R$ decreases monotonically along z [Fig. 9(a)]. Thus, the viscous normal stress *resists* jet stretching everywhere. With extension thinning, T lowers because of the reduced viscosity, and so does $|T'|$ over most of the jet. Hence, stretching is enhanced by extension thinning [Fig. 9(b)].

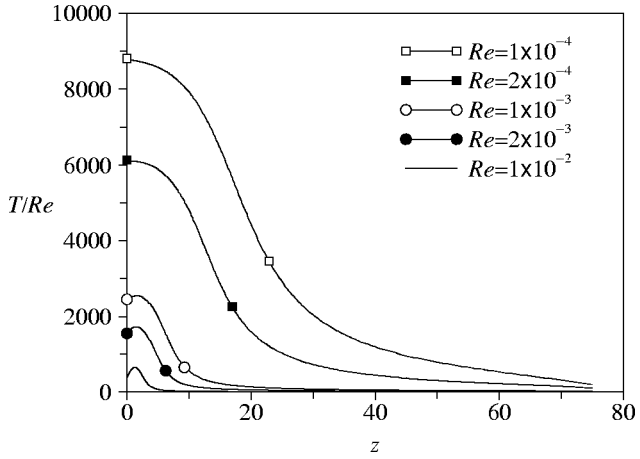

FIG. 10. Profiles of T/Re for the Newtonian solutions in Fig. 6(a) at various Re. Stretching increases with Re for both mildly and severely stretched jets.

As a byproduct of the preceding discussion, we may now explain the effect of Re on a Newtonian jet [cf. Fig. 6(a)]. From Eq. (13), it is T/Re that determines the effect of η_0 on the stretching of a Newtonian jet. Figure 10 shows that the solutions in Fig. 6(a) correspond to mild stretching at low Re and severe stretching at higher Re. For mild stretching, increasing Re lowers T/Re and reduces its downhill slope. For severe stretching, the initial rise in T becomes more pronounced with increasing Re, so much so that $T(z)$/Re assumes a steeper initial upturn. In both cases, therefore, increasing Re intensifies stretching of a Newtonian jet.

2. Extension thickening

We now turn to "humped" $\overline{\eta}$ curves with extension thickening followed by thinning, typical of LDPE melts.[37] We will first study *mild stretching* by using the same parameter values as in Fig. 9, except for the rheological parameters. The power-law indices are fixed at $m=n=0.5$ and two Deborah numbers are tested: De$=\overline{\text{De}}=10$ and De$=\overline{\text{De}}=100$. In both cases, v' falls in the range of 0.09–0.31 [Fig. 11(a)], which produces extension thickening for De$=10$ and extension thinning for De$=100$ (see Fig. 7). The range of the viscosity is roughly the same in the two cases, between 1.8 and 3.8 times the zero-strain-rate value η_0 [Fig. 11(b)]. As a result of the higher $\overline{\eta}$, jet stretching is milder in both cases than a Newtonian jet of viscosity η_0 or a purely extension thinning jet [Fig. 11(c)]. This is consistent with the analysis of Fig. 9; stretching is resisted by a declining T for mildly stretched jets. Furthermore, extension thickening (De$=10$) is more effective than extension thinning (De$=100$) in reducing jet stretching. The reason for this difference is apparent from the almost symmetric shapes of the $\overline{\eta}$ curves. For extension thickening, $\overline{\eta}$ is higher at the upstream part of the jet where most stretching occurs. This leads to a higher tensile force upstream that suppresses jet stretching more effectively.

For a humped viscosity curve, the contrast between severe and mild stretching is not as striking as for the purely

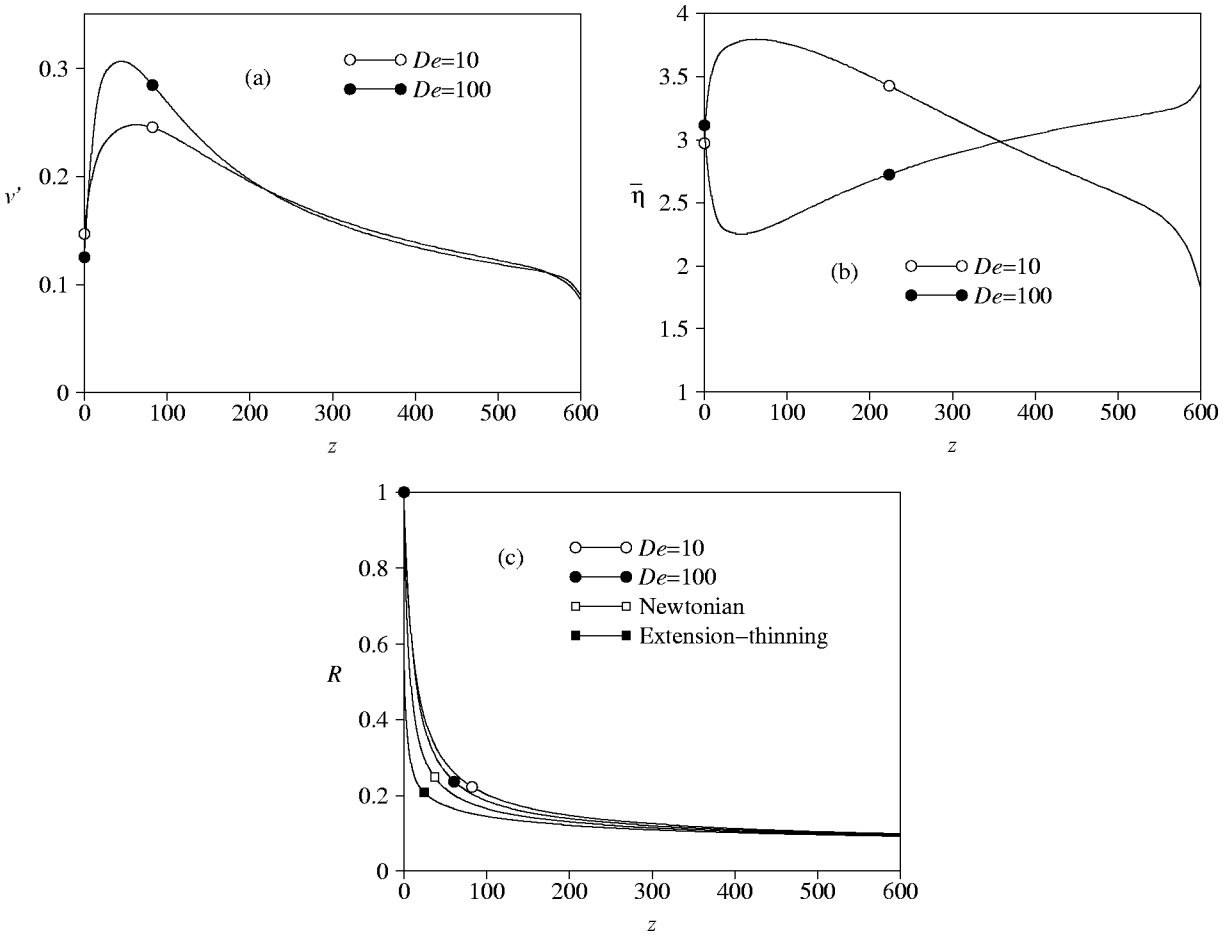

FIG. 11. The effects of a humped viscosity curve on a mildly stretch jet. The parameters are the same as those in Fig. 9 except for the power indices ($m=n=0.5$) and the Deborah number. (a) Strain rate v'; (b) viscosity $\overline{\eta}$; (c) radius R. A Newtonian jet and a purely extension-thinning jet ($n=0.5$, $m=1$, De$=100$) are also shown for comparison.

thinning viscosity in Figs. 8 and 9. In fact, as the hump becomes more prominent, the severe-stretching behavior of Fig. 8 gives way to the mild-stretching dynamics of Fig. 9. To illustrate this transition, we use the parameter values for severe stretching, and reduce m gradually to hunch the viscosity curve [Fig. 12(a)]. This monotonically increases the peak of T as well as the slope $|T'|$ on both sides of the peak [Fig. 12(b)]. More importantly, the downhill portion of the $T(z)$ curve expands and eventually dominates the uphill portion. Then the mild-stretching dynamics prevails. The transition can also be discerned from the thinning curves in Fig. 12(c). The delayed thinning for $m=1$ is characteristic of severe-stretching behavior. As m is decreased to 0.99, the degree of delayed thinning is reduced; stretching is enhanced at the beginning of the jet and reduced farther downstream. This effect is evidently due to the change of T [Fig. 12(b)]. As m lowers to 0.96, the viscosity curve is close to Newtonian in the range of extension rate covered ($1<v'<184$), and the thinning curve $R(z)$ also approaches the Newtonian solution. When m is farther reduced to 0.9, the thinning rate increases at the origin but decreases farther downstream so that the overall thinning is reduced. For even lower m, mild-stretching dynamics dominates; the $R(z)$ curve moves up and away from the Newtonian curve as stretching is lessened by increasing viscosity.

B. Strain hardening

Tirtaatmadja and Sridhar[33] noticed in startup-of-elongation experiments that the stress-growth curves at different strain rates collapse more or less onto a master curve when plotted using the Hencky strain γ. This has inspired us to use an empirical $\overline{\eta}^{+}(\gamma)$ function to represent strain hardening. The following formula is capable of representing the Tirtaatmadja and Sridhar data for PIB-in-PB Boger fluids:

$$\frac{\overline{\eta}^{+}}{3\eta_0}=\begin{cases}\exp\left\{p\left[1-\cos\left(\dfrac{\gamma^2}{\gamma_s^2}\pi\right)\right]\right\}, & \text{if } \gamma\leqslant\gamma_s,\\ \exp(2p), & \text{if } \gamma>\gamma_s,\end{cases} \tag{19}$$

where γ_s is the strain at which a steady-state extensional viscosity is attained, and the parameter p determines the steady-state Trouton ratio. The data of Tirtaatmadja and Sridhar[33] suggest that $\gamma_s\approx 6$ and $p\approx 3.3$. We will explore the effects of strain hardening by varying p with $\gamma_s=6$ fixed, and Fig. 13 plots Eq. (19) for several values of p. Needless to say, Eq. (19) is intended only as a crude representation of the memory effect in a viscoelastic fluid. Besides, concentrated solutions and melts typically exhibit less strain hardening than Boger fluids.

We further assume that the jet exiting the spinneret has a

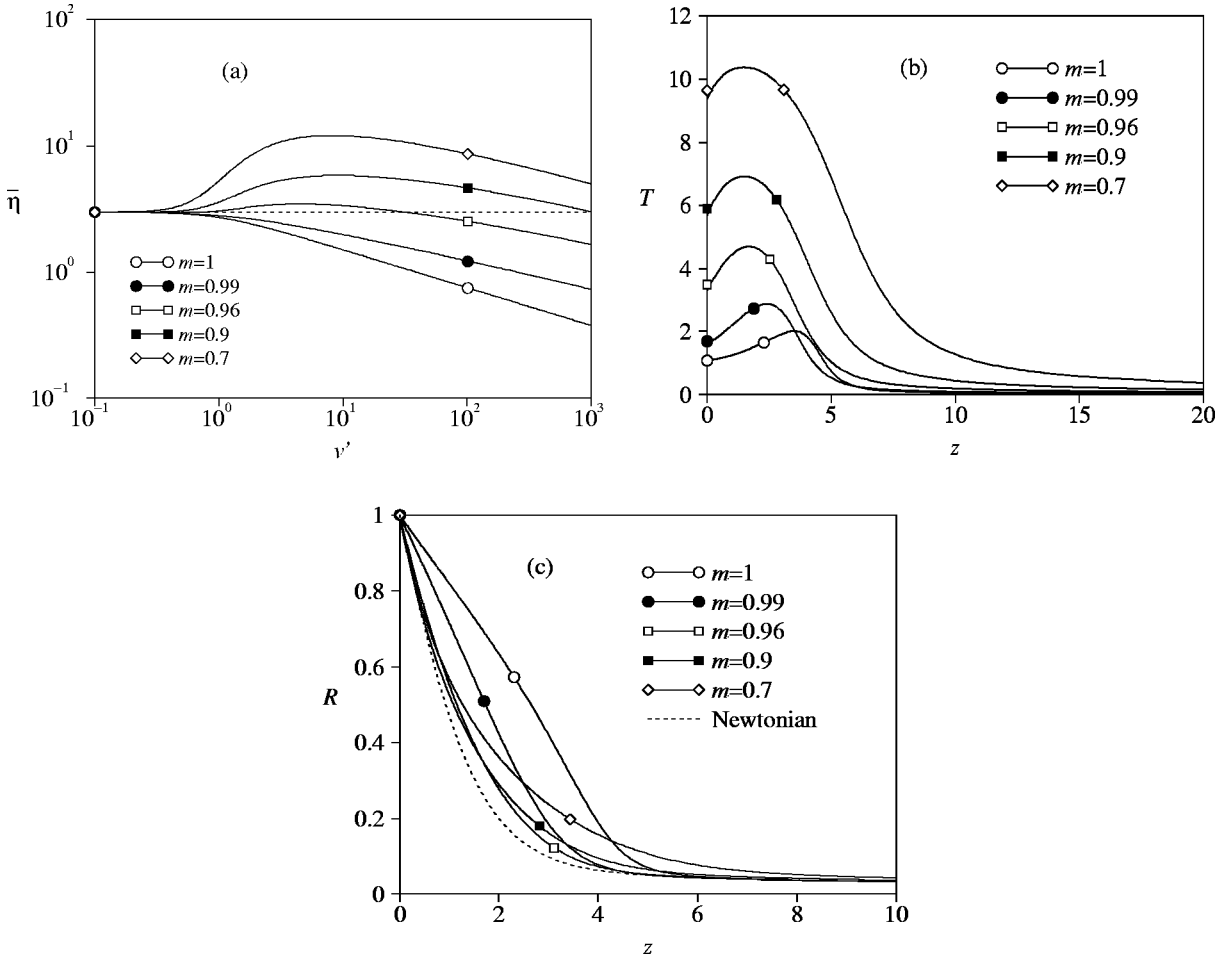

FIG. 12. The effects of a humped viscosity curve on a severely stretch jet. Here $De=\bar{De}=1$, $n=0.7$. The other parameters are the same as in Fig. 8. (a) Viscosity curves for various m values; (b) profiles of the tensile force $T(z)$; (c) stretching curves $R(z)$. The severely stretched Newtonian jet is also shown for comparison.

fixed "prestrain" of $\gamma_0=0.1$. The strain increases along the jet according to

$$\gamma-\gamma_0=\int \dot{\gamma}dt=\int \sqrt{3}v'dt=\int_0^z \sqrt{3}\frac{v'}{v}dz$$

$$=\sqrt{3}\ln v=-2\sqrt{3}\ln R,$$

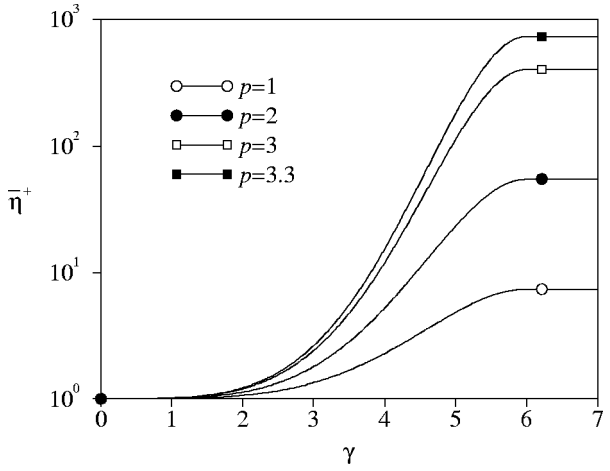

FIG. 13. Strain hardening represented by Eq. (19) for several values of p. The extensional viscosity $\bar{\eta}^+$ is scaled by $3\eta_0$.

where all parameters are dimensionless and $v(0)=R(0)=1$.

Figure 14(a) plots the jet radius for the mild-stretching parameters of Fig. 9 at various degrees of strain hardening. With increasing p, stretching is enhanced initially but weakens downstream. Eventually, *thicker* fibers are produced as a result of strain hardening. This effect can be readily explained by examining the profiles of the tensile force $T(z)$ [Fig. 14(b)]. For mild stretching, T decreases monotonically along z and resists stretching. As a consequence of strain hardening, $\bar{\eta}^+$ increases along z, rapidly at the beginning and plateauing toward $\gamma=\gamma_s$ [Fig. 14(c)]. This has two effects on T. First, the descending slope $|T'|$ is reduced at the beginning of the jet and so initial stretching is enhanced, as seen in Fig. 14(a). Second, the higher level of viscosity after $\gamma>\gamma_s$ produces a larger negative T' for the rest of the jet. Thus, stretching is *dampened* farther downstream. Because of the competing actions in the upstream and downstream portions of the jet, the overall effect on the final fiber radius is remarkably small considering the drastic increase in viscosity caused by strain hardening. For $p=3.3$, the fiber is approximately 60% thicker at the exit than a Newtonian fiber. The more severe initial stretching is accompanied by steeper rises in E and σ for reasons explained in Sec. III B.

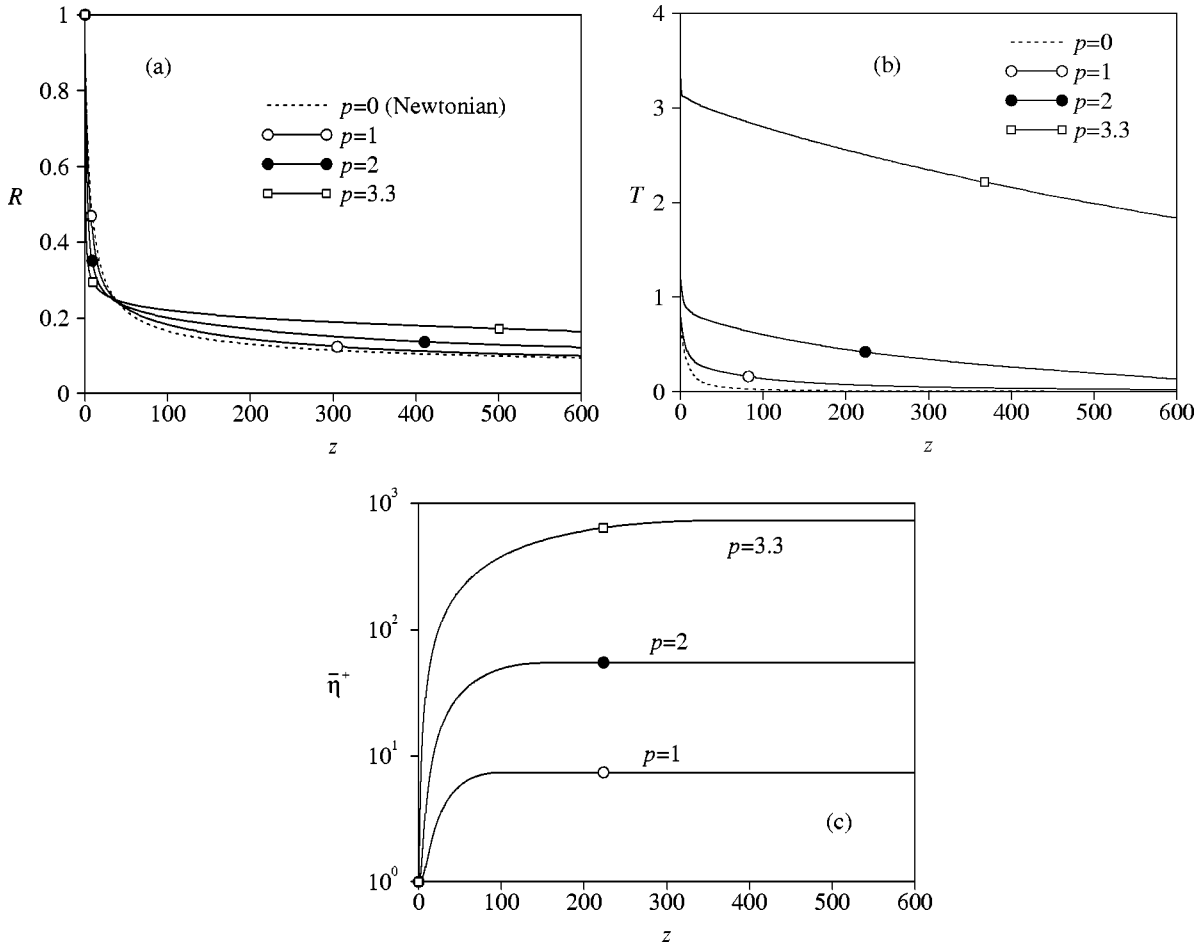

FIG. 14. Effects of strain hardening on the mildly stretched jet. (a) Jet radius R; (b) tensile force T; (c) scaled extensional viscosity $\overline{\eta}^+$.

On the severely stretched jet, strain hardening has similar effects. Stretching is enhanced initially but suppressed farther downstream to produce thicker fibers [Fig. 15(a)]. Strain hardening raises the level of the tensile force everywhere [Fig. 15(b)]. In particular, the rise of T at the start of the jet steepens, resulting in greater initial stretching. The higher peak of T necessitates a more pronounced decline downstream; hence the suppression of stretching over the rest of the jet. In fact, strain hardening can be understood more generally regardless of the hump in T. The initial growth in $\overline{\eta}^+$ implies an increase in T', be it positive or negative; an increasing T will increase more rapidly and a declining T will decline more slowly. This intensifies the initial stretching and sets up the conditions for greater suppression of stretching farther downstream. Thus, strain hardening affects the severely and mildly stretched jets in much the same way.

V. CONCLUDING REMARKS

In this paper, we have introduced non-Newtonian rheology into a theoretical model for electrospinning, and examined the effects of extension thinning, extension thickening, and strain hardening. The results are summarized as follows.

(a) For a purely extension-thinning fluid, mildly and severely stretched jets behave differently. The thinning viscosity enhances stretching for the former and delays stretching for the latter.

(b) For a fluid that extension thickens at lower strain rates and thins at higher strain rates, stretching is hampered by the higher viscosity for both mildly and severely stretched jets.

(c) Strain hardening enhances stretching upstream and suppresses it downstream, and eventually produces thicker fibers.

This work has two limitations. First, the slender-body theory avoids treating the physics near the nozzle directly. Instead, it models the rapid dynamics there by a boundary layer. Though not as intellectually satisfying as a rigorous solution, this model represents experimental observations reasonably well provided that the correct current is input as a parameter. Second, non-Newtonian rheology is incorporated *ad hoc* via empirical expressions for the extensional viscosity. A future task is to incorporate viscoelastic constitutive equations into the electrohydrodynamics of the problem.

ACKNOWLEDGMENTS

This work was supported in part by 3M and the National Science Foundation (NSF). I thank Michael Brenner for

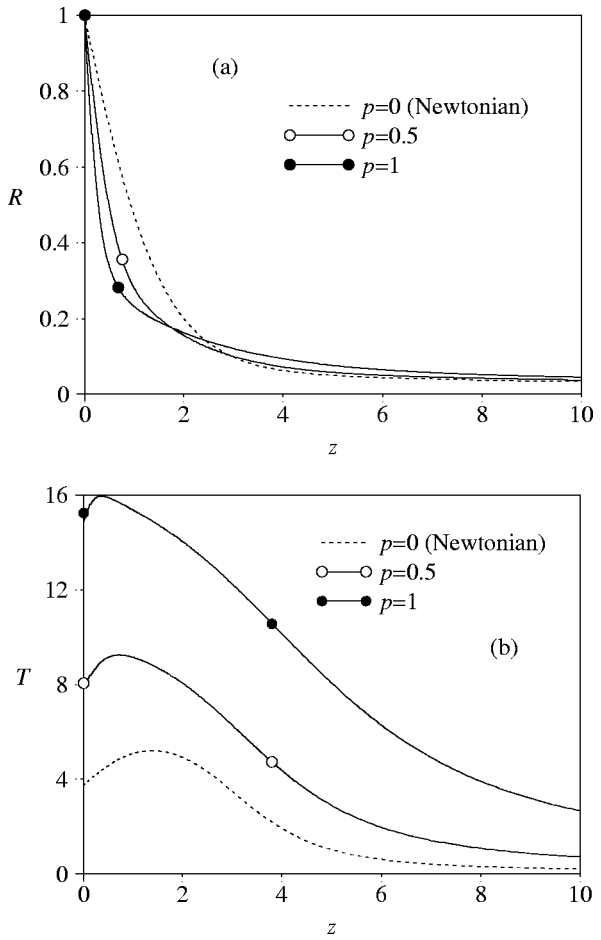

FIG. 15. Effects of strain hardening on the severely stretched jet. (a) Jet radius R; (b) tensile force T.

many insightful comments, and Darrell Reneker and Steve Bechtel for critiquing an earlier version of the paper. I also acknowledge Osman Basaran, Morton Denn, Patrick Mather, and Soemantri Widagdo for stimulating discussions, and Zhen-Su She, Shiyi Chen, and the State Key Laboratory for Turbulence Research at Peking University for hosting a summer visit during which the manuscript was completed. This work was originally presented at the Symposium on Multi-Component and Multiphase Fluid Dynamics, in conjunction with the 14th U.S. National Congress of Applied Mechanics. The Symposium celebrated the pioneering contributions to fluid mechanics by Daniel D. Joseph.

[1]J. Doshi and D. H. Reneker, "Electrospinning process and applications of electrospun fibers," J. Electrost. **35**, 151 (1995).
[2]D. H. Reneker and I. Chun, "Nanometre diameter fibres of polymer, produced by electrospinning," Nanotechnology **7**, 216 (1996).
[3]C. J. Buchko, L. C. Chen, Y. Shen, and D. C. Martin, "Processing and microstructural characterization of porous biocompatible protein polymer thin films," Polymer **40**, 7397 (1999).
[4]M. M. Bergshoef and G. J. Vancso, "Transparent nanocomposites with ultrathin, electrospun nylon-4,6 fiber reinforcement," Adv. Mater. **11**, 1362 (1999).
[5]A. F. Spivak and Y. A. Dzenis, "Asymptotic decay of radius of a weakly conductive viscous jet in an external electric field," Appl. Phys. Lett. **73**, 3067 (1998).
[6]M. M. Hohman, M. Shin, G. Rutledge, and M. P. Brenner, "Electrospinning and electrically forced jets: I. Stability theory," Phys. Fluids **13**, 2201 (2001).
[7]M. M. Hohman, M. Shin, G. Rutledge, and M. P. Brenner, "Electrospinning and electrically forced jets: II. Applications," Phys. Fluids **13**, 2221 (2001).
[8]D. H. Reneker, A. L. Yarin, H. Fong, and S. Koombhongse, "Bending instability of electrically charged liquid jets of polymer solutions in electrospinning," J. Appl. Phys. **87**, 4531 (2000).
[9]A. L. Yarin, S. Koombhongse, and D. H. Reneker, "Bending instability in electrospinning of nanofibers," J. Appl. Phys. **89**, 3018 (2001).
[10]Y. M. Shin, M. M. Hohman, M. P. Brenner, and G. C. Rutledge, "Electrospinning: A whipping fluid jet generates submicron polymer fibers" Appl. Phys. Lett. **78**, 1149 (2001).
[11]D. A. Saville, "Electrohydrodynamics: The Taylor–Melcher leaky dielectric model," Annu. Rev. Fluid Mech. **29**, 27 (1997).
[12]M. M. Denn, C. J. S. Petrie, and P. Avenas, "Mechanics of steady spinning of a viscoelastic liquid," AIChE J. **21**, 791 (1975).
[13]A. M. Ganan-Calvo, "On the theory of electrohydrodynamically driven capillary jets," J. Fluid Mech. **335**, 165 (1997).
[14]S. E. Bechtel, C. D. Carlson, and M. G. Forest, "Recovery of the Rayleigh capillary instability from slender 1-D inviscid and viscous models," Phys. Fluids **7**, 2956 (1995).
[15]J. Eggers, "Nonlinear dynamics and breakup of free-surface flows," Rev. Mod. Phys. **69**, 865 (1997).
[16]E. J. Hinch, *Perturbation Methods* (Cambridge University Press, New York, 1991), p. 43.
[17]J. Eggers and T. F. Dupont, "Drop formation in a one-dimensional approximation of the Navier–Stokes equation," J. Fluid Mech. **262**, 205 (1994).
[18]X. Zhang, R. S. Padgett, and O. A. Basaran, "Nonlinear deformation and breakup of stretching liquid bridges," J. Fluid Mech. **329**, 207 (1996).
[19]R. Keunings, M. J. Crochet, and M. M. Denn, "Profile development in continuous drawing of viscoelastic liquids," Ind. Eng. Chem. Fundam. **22**, 347 (1983).
[20]M. M. Denn, "Fibre spinning," in *Computational Analysis of Polymer Processing*, edited by J. R. A. Pearson and S. M. Richardson (Applied Science, New York, 1983), Chap. 6.
[21]V. N. Kirichenko, I. V. Petryanov-Sokolov, N. N. Suprun, and A. A. Shutov, "Asymptotic radius of a slightly conducting liquid jet in an electric field," Sov. Phys. Dokl. **31**, 611 (1986).
[22]R. P. A. Hartman, D. J. Brunner, D. M. A. Camelot, J. C. M. Marijnissen, and B. Scarlett, "Electrohydrodynamic atomization in the cone-jet mode physical modeling of the liquid cone and jet," J. Aerosol Sci. **30**, 823 (1999).
[23]A. M. Ganan-Calvo, "Cone-jet analytical extension of Taylor's electrostatic solution and the asymptotic universal scaling laws in electrospraying," Phys. Rev. Lett. **79**, 217 (1997); erratum **85**, 4193 (2000).
[24]R. Jaeger, M. M. Bergshoef, C. Martin I. Batlle, and G. J. Vancso, "Electrospinning of ultra-thin polymer fibers," Macromol. Symp. **127**, 141 (1998).
[25]J. M. Deitzel, J. Kleinmeyer, D. Harris, and N. C. Beck Tan, "The effect of processing variables on the morphology of electrospun nanofibers and textiles," Polymer **42**, 261 (2001).
[26]*CRC Handbook of Chemistry and Physics*, 62nd ed. (CRC Press, Boca Raton, 1981).
[27]W. H. Press, S. A. Teukolsky, W. T. Vetterling, and B. P. Flannery, *Numerical Recipes in FORTRAN 77*, 2nd ed. (Cambridge University Press, New York, 1992).
[28]G. Kortüm and J. O'M. Bockris, *Textbook of Electrochemistry* (Elsevier, New York, 1951), p. 618.
[29]K. Cruse, "Elektrische Leitfähigkeit reiner Flüssigkeiten," in *Eigenschaften der Materie in ihren Aggregatzuständen*, 7. Teil (Springer-Verlag, Berlin, 1960), Sec. 2762.
[30]J. A. Dean, *Lange's Handbook of Chemistry*, 13th ed. (McGraw-Hill, New York, 1985), pp. 6-37.
[31]A. M. Ganan-Calvo, "The surface charge in electrospraying: its nature and its universal scaling laws," J. Aerosol Sci. **30**, 863 (1999).
[32]D. F. James and K. Walter, "A critical appraisal of available methods for the measurement of extensional properties of mobile systems," in *Techniques in Rheological Measurements*, edited by A. A. Collyer (Elsevier, London, 1993).
[33]V. Tirtaatmadja and T. Sridhar, "A filament stretching device for measurement of extensional viscosity," J. Rheol. **37**, 1081 (1993).
[34]W. N. Song and Z. M. Xia, "A phenomenological viscosity model for

polymeric fluid,'' J. Non-Newtonian Fluid Mech. **53**, 151 (1994).
[35]R. B. Bird, C. F. Curtiss, R. C. Armstrong, and O. Hassager, *Dynamics of Polymeric Liquids, Vol. 1. Fluid Mechanics* (Wiley, New York, 1987), p. 170.
[36]H. M. Laun and H. Münstedt, ''Elongational behavior of a low density polyethylene melt,'' Rheol. Acta **17**, 415 (1978).
[37]R. J. Fisher and M. M. Denn, ''A theory of isothermal melt spinning and draw resonance,'' AIChE J. **22**, 236 (1976).